Role of Convective Processes in the Development of the Low-Level Jet

CHAING CHEN, WEI-KUO TAO, AND STEPHEN LANG
Mesoscale Atmospheric Processes Branch, Laboratory for Atmospheres, NASA/GSFC, Greenbelt, Maryland

Abstract

Numerical simulations were conducted using a two-dimensional, nonhydrostatic model in order to determine the mechanism responsible for the development of the low-level jet (LLJ). In their three-dimensional model simulations of a Mei-Yu front occurred over southeastern China and Taiwan during the early summer of 1991, Chen et al. (1996) found that the development of the LLJ is sensitive to the presence of convective cloud processes. In this paper, we use an idealized two-dimensional model to verify their findings. We impose the confluent or the shear forcing on upper-level fronts and examine the response of the frontal forcing in producing the ageostrophic secondary circulation which can subsequently initiate the convection. Once the convection develops, the generation of inertia-gravity waves can lead to the development of the LLJ. The importance of the LLJ is in its ability to transport moisture to maintain the convective system. We found that in order to produce a quasi-steady state convective system, a moisture gradient in the along frontal direction needs to be specified in the simulation.

1 Introduction

The study of the southwesterly LLJ, that occurs to the south of the Mei-Yu front between 700 and 850 hPa, has been an important topic since heavy precipitation is statistically closely related to its existence. In the past, the mechanism responsible for the development of the LLJ has been explored by many investigators. For instance, Matsumoto (1973), and Ninomiya and Akiyama (1974) suggested that the LLJ developed via the downward mixing of momentum by convection. Hsu and Sun (1994) suggested that the stratiform cloud could lead to the development of the LLJ by creating a low-level pressure trough. Chen et al. (1994), and Chen and Chen (1995), on the other hand suggested that the intensification of the LLJ is linked to the deepening of the midlatitude cyclone.

In their study using the Penn State/NCAR MM5 mesoscale model, Chen et al. (1996) found that the presence of convective cloud processes played an important role in the intensification of the LLJ. In their study, the onset of the convection is triggered by the divergence of the ageostrophic flow at upper-levels. The development of this ageostrophic flow, moving across from the warm side to the cold side of the upper-level jet, is produced by the thermal wind adjustment process wherein frontal forcing is acting upon the upper-level front. Once the convection is triggered, an indirect circulation with sinking motion to the south can lead to the development of the LLJ.

A similar finding was also reported by Chou et al. (1990). They found that convective heating could generate a 'reversed Hadley' circulation with rising motion in the convective region and sinking motion equatorward. The LLJ is produced by the Coriolis acceleration of the return flow in the lower branch of the circulation. Moreover, in his theoretical work, Chen (1982) demonstrated that by including convective heating, the thermal wind adjustment process could generate two circulations with the region of convective heating centered between these two circulations. The low-level return flow of the right hand circulation is responsible for the generation of the LLJ.

In this paper, we use a two-dimensional, nonhydrostatic model to test Chen et al.'s (1996) finding, that the thermal wind adjustment process associated with the the upper-level frontal forcing can lead to the development of the LLJ. In order to activate the thermal wind adjustment process, two different frontal forcings (confluent and shear) are applied individually to an upper-level front. In section 2, we describe and highlight features of the model and initial conditions. In section 3, we present the results and explain how the frontal forcing induces secondary circulations through the thermal wind adjustment process. We then introduce the moisture and the moisture gradient at low-levels to examine processes that

are responsible for the generation of convection and the development of the LLJ. Finally, a summary is presented in Section 4.

2 Model and initial conditions

The two-dimensional nonhydrostatic model used in this study is described by Chen (1991). It uses spatial finite differencing and a time-splitting scheme to solve four prognostic equations on a staggered C grid. Following Reeder and Smith (1987), the model is initialized by specifying an upper-level jet (Fig. 1a) in the model domain. The initial profile of the potential temperature (Fig. 1b) associated with the front is then reconstructed from the thermal wind equation. Therefore, the front is initially geostrophically balanced.

To drive the frontogenesis process during the simulation, we use either shear or confluent forcing which is achieved by prescribing an along-front temperature gradient ($\partial\theta/\partial y$) or a cross-front geostrophic wind gradient ($\partial u_g/\partial x$). To eliminate the generation of spurious gravity waves as reported by Orlanski and Ross (1977), we increased these gradients ($\partial\theta/\partial y$ or $\partial u_g/\partial x$) gradually. We found that this method is quite robust and convenient to use. The spinup procedure is an alternative to the application of the Sawyer-Eliassen equation as described by Reeder and Smith (1987). The advantage of using the spinup procedure can be seen as follows: (a) the Sawyer-Eliassen (S-E) equation becomes invalid and has a singularity in the solution when there is negative potential vorticity; (b) the S-E equation does not include the effect of latent heat release; and (c) solving the S-E equation becomes complicated when terrain and surface friction effects are considered.

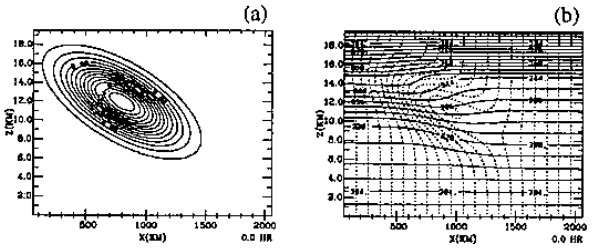

Figure 1: *Contours of initial (a) along front wind (v, m s^{-1}) and (b) θ (solid, K) and $M = fx + v$ (dashed, every 5 m s^{-1}) for the upper-level front.*

The model has 258 grid points in the horizontal (x) direction and 100 points in the vertical (z) direction. It has a rigid lid at the top and radiative conditions on the lateral boundaries. The bottom boundary condition is free-slip and is thermally insulated (no heat flux through the bottom boundary). The grid resolution is $\Delta x = 20$ km and $\Delta z = 200$ m; the time step is $\Delta t = 10$ s. Also in this study, we use $f = 5 \times 10^{-5}$ s^{-1}, $\partial\theta/\partial y$ = -0.25 K/100 km (shear forcing case) and $\partial u_g/\partial x = -10^{-5}$ s^{-1} (confluence forcing case).

The model is initialized by a stable stratified standard atmosphere with a temperature lapse rate of 6.5 K km^{-1} ($N^2 = 10^{-4}$ s^{-2}) below the height of 15 km for which the surface potential temperature is 296 K. Above that height, we use a lapse rate of $N^2 = 3 \times 10^{-4}$ s^{-2}.

When moisture is included in the simulation, the microphysical package developed by Tao and Soong (1986) and Tao and Simpson (1993) is used to account for convective cloud processes. In order to demonstrate the mechanism that produces slantwise convection in this study, no cumulus parameterization scheme is incorporated to release the subgrid convective instability in the vertical direction. Since a large grid spacing is used in simulations, the mechanism to generate hail is not allowed. Only the formation of cloud water, rain, cloud ice, snow and graupel is permitted.

One may question the validity of using the cloud microphysical scheme in simulations with a coarse grid resolution. Our justification is based on the fact that the convective system reported by Chen et al. al (1996) has a scale of 150 $\sim$ 200 km. Therefore, a 20 km grid resolution may be good enough to resolve this system. In addition, we found that the model is able to release the atmospheric potential instability despite a coarse grid resolution is used. Therefore, we chose to use such a grid in conjunction with explicit cloud processes to reveal the atmospheric response to the diabatic heating. We also conducted tests by applying a time independent heating function in the middle of the model domain to examine main characteristics of internal gravity waves.

3 Results

In this paper, we explore the processes that are important and that can lead to the development of the LLJ. Based on the finding reported by Chen et al. (1996), we concentrate our attention on determining the role of the convection in producing the LLJ. In order to understand the onset of the convection, we also explore how the ageostrophic secondary circulation, induced by frontal forcing through the thermal wind adjustment process, can provide a favorable environment for promoting the convection.

3.1 Development of the Ageostrophic Secondary Circulation

By using quasi-geostrophic theory in a two-dimensional domain (x-z), Hoskins et al. (1978)

demonstrated that thermal wind balance could be destroyed by its own geostrophic motion which originally was thermal wind balanced, i.e.,

$$(\frac{\partial}{\partial t}+\tilde{V}_g\cdot\nabla)(\frac{g}{\theta_0}\frac{\partial\theta}{\partial x}) = -(\frac{\partial}{\partial t}+\tilde{V}_g\cdot\nabla)f(\frac{\partial\tilde{V}_g}{\partial z}) = Q \quad (1)$$

where

$$Q = -(\frac{g}{\theta_0}\frac{\partial\tilde{V}_g}{\partial x})\cdot\nabla\theta, \quad (2)$$

and

$$\tilde{V}_g = (u_g, v_g).$$

Through advective processes, the geostrophic flow brings changes to $(g/\theta_0)(\partial\theta/\partial x)$ and $(f)(\partial v_g/\partial z)$ equally in magnitude but opposite in sign. Therefore, the geostrophic flow is no longer thermal wind balanced.

For instance, at the upper-level jet entrance area, we may have a confluence of u_g (i.e., $\partial u_g/\partial x < 0$) acting on a horizontal potential temperature gradient ($\partial\theta/\partial x > 0$) (upper-level front, Fig. 2a). According to (1), the destruction of the thermal wind balance is manifested by the fact that there is an increase in temperature gradient ($\partial\theta/\partial x$) and a decrease in wind shear ($\partial v_g/\partial z$) at the upper-level front because $Q = -(g/\theta_0)(\partial u_g/\partial x)(\partial\theta/\partial x) > 0$ (Fig. 2b). In order to restore the thermal wind balance, a negative ageostrophic flow u_{ag} has to develop above the region where $Q > 0$ (Fig. 2d). Subsequently, the normal wind speed v_g and shear $\partial v_g/\partial z$ will be increased through Coriolis turning of u_{ag}.

Another way to achieve thermal wind balance is through the adiabatic warming and cooling processes associated with lifting and subsiding the air mass along the right and left sides of the jet (facing jet downstream) below the height of 12 km. The convergence and divergence of Q as shown in Fig. 2c indicates the region to have rising and sinking motion, respectively. This rising motion, transverse ageostrophic flow, and sinking motion as shown in Fig. 2d constitute the major part of the circulation in the troposphere. To complete the circulation, a return flow at low-levels develops in response to the generation of the isallobaric wind or the increase of the pressure gradient force in the transverse direction. This pressure gradient force is induced dynamically by the convergence and divergence of air associated with the corresponding sinking and rising motion that is located on the two sides of the circulation (Uccellini and Johnson 1979).

3.2 Development of the Upright Convection

The simulation to test the mechanism responsible for producing the ageostrophic motion in the previous section does not include moisture. In this section, we are interested in finding out the role of the ageostrophic circulation in triggering convection. Therefore, a moisture pool is introduced on the right hand side of the domain at the beginning of the simulation. The relative humidity in the moisture pool is about 95% from the surface to z = 10 km. The relative humidity is about 40% outside the moisture pool. In addition, there is no moisture at heights above 10 km. The model is then integrated by using the same frontal forcing as described in the previous section (confluent forcing). After 12 hours of integration, as shown in Fig. 3 the development of a similar ageostrophic flow (compared to Fig. 2d) is visible. Though small in magnitude, there is a rising motion that develops inside the moisture pool. We are interested in knowing whether this small rising motion can induce convection at a later time.

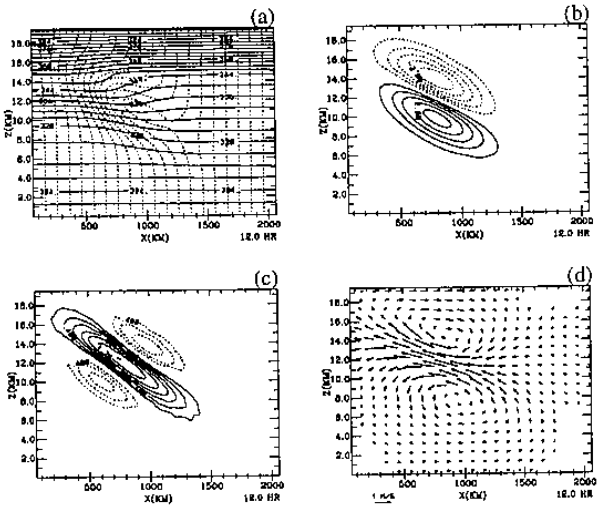

Figure 2: *Cross sections of an upper-level front interacting with confluent frontal forcing at t = 12 hrs of (a) θ (solid, K) and M = fx + v (dashed, every 5 m s^{-1}), (b) Q vector (10^{-12} s^{-3}), (c) $-\partial Q/\partial x$ (10^{-19} cm^{-1} s^{-3}) and (d) ageostrophic wind vectors.*

Fig. 4 shows the time evolution of the cloud and the associated ageostrophic flow field. As evidenced by Fig. 4a, the continuously imposed small rising motion, associated with the thermal wind adjustment process, can indeed trigger convection at mid-levels at t = 26 hrs. Once the initial cloud developed, the vertical development of the convection becomes vigorous (Fig. 4b). Because the atmosphere is excited by the explosive development of the convection, internal gravity waves are found to be generated, and they propagate outward away from the convection at a speed of 20 m s^{-1}. As can be seen in Figs. 4b, 4c and 4d, this outward propagation of internal gravity waves is manifested in the form of rotors produced

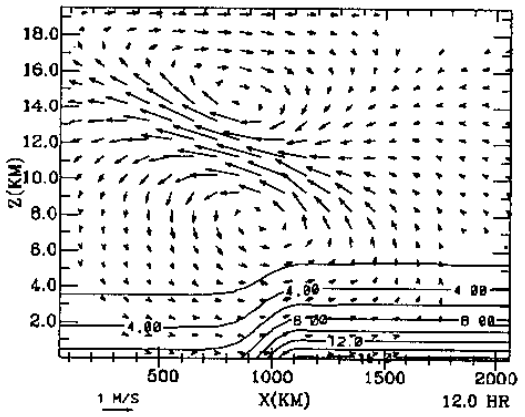

Figure 3: *As in Fig. 2d except with the inclusion of the moisture pool (mixing ratio, gm kg^{-1}).*

on both sides of the convection.

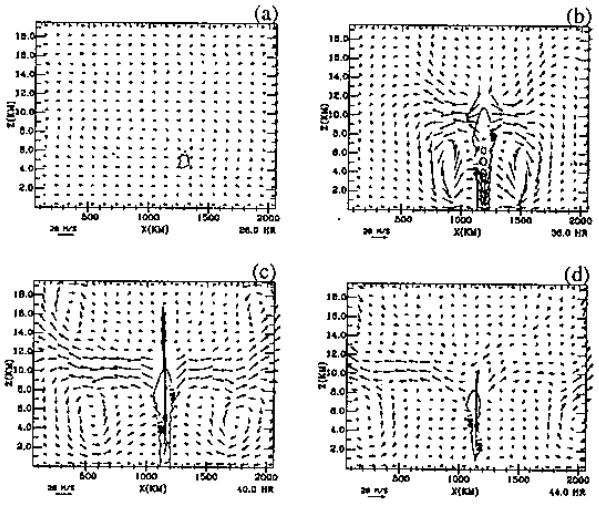

Figure 4: *Cross sections of the cloud field (g kg^{-1}) and wind vectors for the upper-level front with confluent forcing at t = (a) 26, (b) 36, (c) 40 and (d) 44 hrs.*

Although the frontal secondary ageostrophic circulation can induce convection, the development of the convective system appears to burst from the low-level moisture pool and not long lasting. The time span for the entire convective life cycle is about 20 hrs. The reason for this episodic development of the convection may be due to the fact that the CAPE (Convective Available Potential Energy) of the atmosphere is exhausted after the convection. Therefore, the further development of the convection can not be sustained.

3.3 Generation of internal gravity waves

In order to further examine the nature of internal gravity waves as shown in Fig. 4, we conducted additional tests by applying a constant heat source to the same atmosphere in the middle of the model domain. In the testing, no upper-level front and and no frontal forcing were used. In addition, in order to simplify the problem, Coriolis force is not applied. The time independent function of this heat source is specified as follows

$$S(x,z) = \frac{\theta_0}{c_p T_0} S_0 \, exp\left[-\left(\frac{x-x_0}{L_x}\right)^2\right] sin\left(\frac{\pi z}{L_z}\right), \quad for \; z \leq L_z, \tag{3}$$

where x_0 is the location of the heat source. The horizontal width and the vertical depth of the heat source are given as $L_x = 100$ km, $L_z = 10$ km. The strength of the heating is represented by S_0. In the following tests, two types of S_0 were used, i.e., $S_0 = 3 \times 10^4$ (case in Figs. 5a and 5b) and 1.5×10^4 cm^2 s^{-3} (case in Figs. 5c and 5d), which are equivalent to 30 and 15 mm hr^{-1} rainfall rate (Wang et al. 1996) at the surface, respectively.

As shown in Fig. Fig. 5, both strong and weak heating cases produced rotors similar to that shown in Fig. 4. In addition, from the super-imposed isentropes, solitary waves of depression (Rottman and Einaudi 1993) can be identified to propagate away from the heat source. The speed of the rotor or the solitary wave for the strong heating case is about 33 m s^{-1}, while that of the weak heating case is 22 m s^{-1}. Since the speed of the rotor or the solitary wave is sensitive to the magnitude of the heating, we believe that the slower wave speed shown in Fig. 4 reflects the fact that the integral strength of the heating is weaker when the convection is developed in a burst mode.

We also tried other case by adding a Rayleigh friction layer, located between 15 and 20 km, to damp out the upward propagation of gravity waves. The result (not shown) did not suggest a major impact to the generation of solitary waves below 10 km, however, the waves above 15 km were suppressed. We also tried to put back the Coriolis force in the simulation. The result (not shown) indicates that the strength of rotor circulation is slightly weaker than that in Figs. 5a and 5b. With the inclusion of the Coriolis force, the system is able to retain more heat since the temperature of the convective core at 10 km is warmer than the case without Coriolis force activated.

As point out by Lindzen and Tung (1976), the phase speed of internal waves, propagating in a fluid

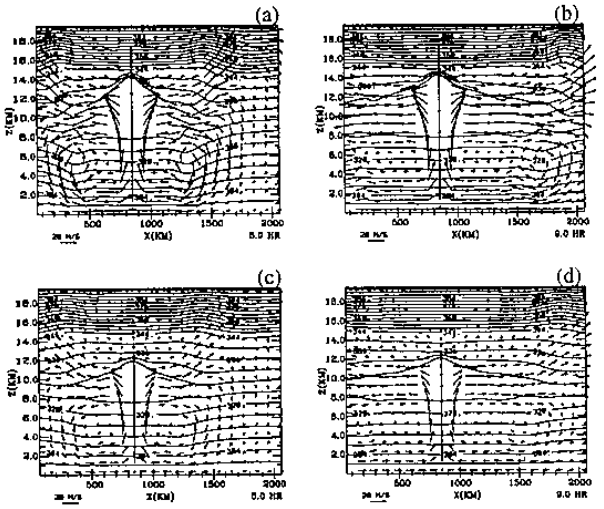

Figure 5: *Cross sections of the potential temperature (θ, k) and wind vectors for case driven by time independent heating function ($Q_0 = 3 \times 10^4$ cm^2 s^{-3}) at t = (a) 5 and (b) 9 hrs. Panels (c)-(d) are as in (a)-(b) except for $Q_0 = 1.5 \times 10^4$ cm^2 s^{-3}.*

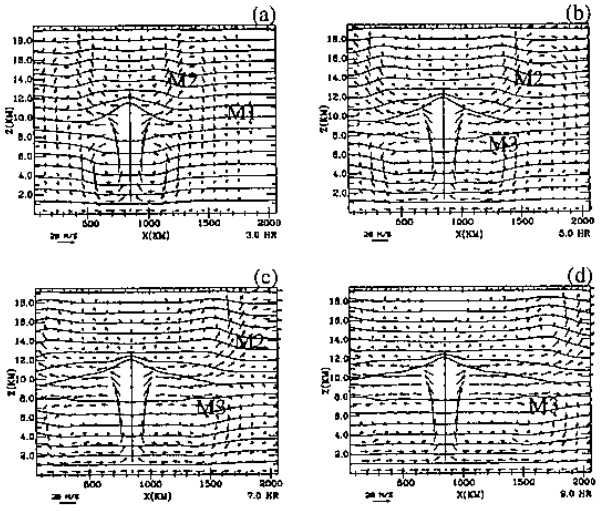

Figure 6: *Cross sections of the potential temperature (θ, k) and wind vectors for case with uniform stability N at t = (a) 3, (b) 5, (c) 7 and (d) 9 hrs. The strength of the heating function is $Q_0 = 1.5 \times 10^4$ cm^2 s^{-3}. Locations of three internal gravity wave modes are marked by M1, M2 and M3. The characteristics of these waves are described in the text.*

of an uniform stability N bounded between two rigid lid with a depth of H, is represented by

$$C_n = \frac{NH}{\pi(1/2+n)}, \quad n = 0, 1, 2, ... \qquad (4)$$

where n is the vertical wave number. For N = 0.01 s^{-1} and H = 20 km, the wave phase speeds for the first three modes are 127, 42 and 25 m s^{-1}, respectively.

In order to verify the wave speed as described by (4), we reran the model with uniform stability and weak heating rate ($S_0 = 1.5 \times 10^4$). The time evolution of internal gravity waves of this case is shown in Fig. 6, in which the leading edge of mode 1, 2 and 3 (n=0,1,2) waves is marked by M1, M2 and M3, respectively. In general, the M1 wave is characterized by the subsidence through out the entire depth of the fluid. The M2 wave has a structure of upward/downward motion in the upper/lower half of the model domain. Lastly, the M3 wave has a structure of down/up/down motions from top to bottom of the model domain. The rotor that we are interested is associated with the M3 wave. The phase speed for M2 wave is about 40 m s^{-1}, while that for M3 is 23 m s^{-1}. The magnitude of these phase speeds agrees very well with that represented by (4).

We also conducted additional tests by using a shallower heating profile. The model response (not shown) of this heating is to produce shallower rotors with a slower speed. The associated wave number for rotors is higher than that shown in Fig. 6. Therefore, the atmosphere choses its dominant mode based on the depth of the heating profile. The result reported by Mapes (1993) indicates that his dominant waves is modes 1 and 2. The reason to produce this lower mode waves is because of a deep heating profile used in in his simulations.

In summary, results shown in this section clearly demonstrate that rotors generated by the case shown in Fig. 4 are reasonable and can be explained by internal gravity wave equations. It is interesting to note that the outward propagation of solitary waves can not generate new convection. The conventional wave-CISK mechanism seems to be not applicable in our case. We noticed that the outward propagation of heat associated with internal gravity waves may lead to the reduction of relative humidity after the passage of waves. This may be the cause to prevent the the generation of new convection.

3.4 Development of the LLJs

In the development of Mei-Yu fronts, the presence of a southwesterly LLJ is a necessary condition. The significance of the LLJ is in its ability to transport moisture northward to maintain the frontal convective system. Therefore, in this section, we will explore the mechanism responsible for the development of the LLJ. Hereafter, the conventional southwesterly LLJ mentioned in Mei-Yu front studies is represented by the westerly LLJ in our idealized simulations.

The outward propagation of internal gravity waves can produce LLJs (both easterly and westerly). Fig. 7

shows the time sequence of the along front wind (or normal wind, V) component. Before the onset of the convection (Fig. 7a), there are no LLJs. Instead, the initially specified westerly jet (V > 0) located at upper levels is the main feature. However, once the convection developed, contours of V wind began to change (Fig. 7b). There is a descending of the upper-level westerly jet to a lower altitude. There is also an upper-level easterly jet that develops to the south (right) side of the convection. In addition, there are a pair of jets (easterly and westerly) that develop at low levels on either side (left and right) of the convection.

Furthermore, Figs. 7c and 7d show that the system is characterized by a horizontal expansion of the low-level easterly and westerly jet (as well as upper-level jets). Comparing with Figs. 4c and 4d, it is not difficult to see that this expansion of LLJs is directly associated with the outward propagation of internal gravity waves or rotors. The entire scenario began with the development of the convection. Subsequently, internal gravity waves were excited, modulated by the Coriolis force, and behaved as inertia-gravity waves. Therefore, LLJs were produced by the Coriolis turning of the returning flow which was a branch of the rotor circulation that propagated outward away from the convection.

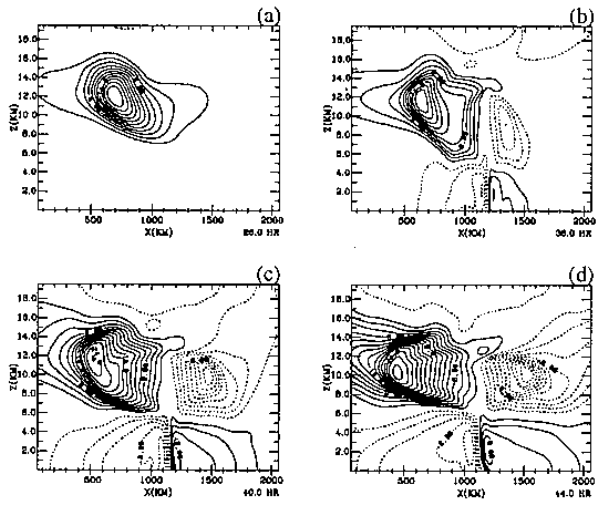

Figure 7: *As in Fig. 4 except for the along front wind (v, m s^{-1}).*

3.5 Development of the Slantwise Convection

Although confluent frontal forcing can induce convection in our idealized 2D simulations, the convective system shown in Fig. 4 is mainly characterized by upright convection. This result is different from that reported by Chen et al. (1996), in which they showed that the cloud system consists of a deep convective cloud and a relatively shallow cloud that extends from the surface up to middle levels in a slantwise direction. In order to produce slantwise convection in our idealized simulations, we have tried many approaches including tests using different frontal forcing and initial temperature and moisture profiles. None of these tests worked. Exploring the results of Chen et al. (1996), we began to examine the role of the along frontal moisture gradient ($\partial q_v/\partial y$). We found that the inclusion of $\partial q_v/\partial y$ in the simulation is crucial for producing a slantwise convective structure.

Fig. 8 shows the development of the upright and slantwise convection when $\partial q_v/\partial y$ is included in the simulation. This $\partial q_v/\partial y$ has a minimum value of -1 gm kg^{-1} per 100 km at the surface and decreases linearly to zero at the height of 4 km. Like that shown in Fig. 4, this case also generates the outward propagation of rotors (Fig. 8a). Unlike that shown in Fig. 4, this case can produce slantwise convection that develops to the right side of the upright convection from the surface up to z = 5 km at t = 52 hrs (Fig. 8b). The tilted wind vectors from low- to mid-levels evidences the development of such a slantwise structure.

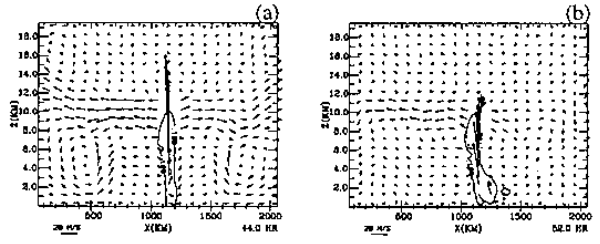

Figure 8: *As in Fig. 4 except for the case with $\partial q_v/\partial y$ = -1 gm kg^{-1} included in the simulation. The result is displayed at t = (a) 44 and (b) 52 hrs.*

Longer time integrations were also carried out. The results (not shown) indicate that the convective system for the case with $\partial q_v/\partial y$ included can last for a long time and is in a quasi-steady state mode, though the system may experience periodical up and down cycles in its convective strength. In contrast, the convective system shown in Fig. 4 dissipates very quickly after t = 44 hrs, and the system is in a burst mode.

It is noted that during the 'quasi-steady state' as shown in Fig. 8b, the northward (left) bound circulation is stronger and extends farther than that of the southward (right). The reason for this stronger northward bound circulation is not clear in this study. The interaction between the convection and the large scale frontal forcing may be the cause. It is also noted that the southward bound circulation, often referred

to as the 'reversed Hadley' circulation in the study of Mei-Yu fronts (Chou et al. 1990), has a horizontal length scale of about 400 $\sim$ 500 km which is about the same as that reported by Chen et al. (1996). Furthermore, this scale is also consistent with the Rossby deformation radii which is given by $\lambda_R = C/f$, where $C \simeq 20$ m s^{-1} and $f = 5 \times 10^{-5}$ s^{-1}.

Fig. 9 shows the corresponding contours of the along front wind (V). Similar to that shown in Fig. 7, the outward propagation of the inertia-gravity waves is responsible for the generation of the upper-level the lower-level jets. It is noted that the orientation of the LLJs shown in Fig. 9a is vertically erect. However, after the slantwise convection develops at t = 52 hrs, Fig. 9b shows that the orientation of the LLJs becomes tilted. This tilted LLJ structure implies that the trajectory of the low-level return flow follows a slantwise pathway.

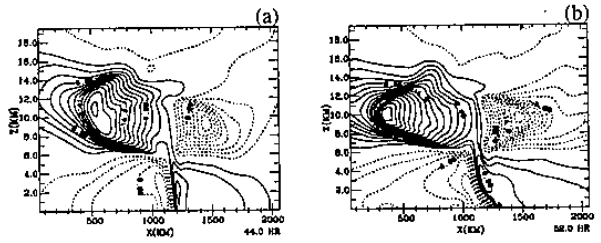

Figure 9: *As in Fig. 8 except for the along front wind (v, m s^{-1}).*

With the inclusion of a negative $\partial q_v/\partial y$, the model response is to produce a moistening (drying) of the air mass at low levels to the right (left) side of the convection because of the ability of the corresponding westerly (easterly) LLJ to replenish (deplete) moisture. Therefore, the air mass at low levels to the right side of the convection will become saturated more easily than that to the left side. Consequently, new shallow convective cells tend to develop in an area adjacent to the right side of the deep upright convection.

The westerly LLJ does not lie directly underneath the deep upright convection. The trajectory of the moist air, advected in by the westerly LLJ, follows a slantwise path toward the main deep upright convection. The tilted structure of the absolute momentum surface at low levels (caused by the tilting of the V profile) is the reason that the air parcel moves in a slantwise direction. This might appear to be a 'chicken and egg' problem, however, we felt that the tendency to produce the shallow convection to the right side of the upright convection is the main contributing factor that can lead to the final establishment of the slantwise convection.

3.6 Role of the Shear Frontal Forcing

The thermal wind adjustment process can also become active when there is a potential temperature gradient in the normal wind direction ($\partial\theta/\partial y$) interacting with the v_g jet ($Q = -(g/\theta_0)(\partial v_g/\partial x)(\partial\theta/\partial y)$). For instance, in Fig. 10a, we have a $v_g > 0$ jet located at upper-levels with a north/south temperature gradient $\partial\theta/\partial y < 0$. Therefore, the differential advection of warm air associated with the v_g jet can change temperature gradients on both sides of the jet. As shown in Fig. 10b, there is an increase ($Q > 0$) and decrease ($Q < 0$) in $\partial\theta/\partial x$ to the left and the right side of the jet, respectively. The thermal wind response to these temperature changes is to generate a positive and a negative ageostrophic flow (Fig. 10d) above the region where $Q > 0$ and $Q < 0$, respectively. Another response is to generate rising motion at the center of the jet and sinking motion along both sides. The convergence/divergence pattern of the Q vector shown in Fig. 10c depicts the regions having rising and sinking motion quite well.

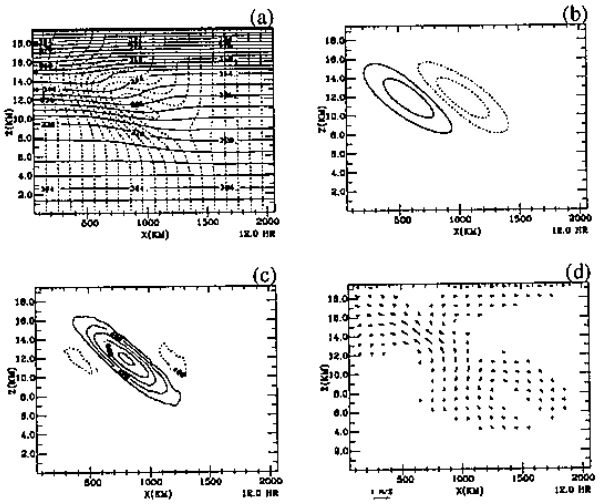

Figure 10: *As in Fig. 2 except for the case with shear frontal forcing.*

Like that shown in Fig. 2 of the confluent case, the frontal shear forcing induced ageostrophic rising motion near the surface is also weak. The same procedure is then applied introducing a moisture pool to test whether this small rising motion can trigger convection or not. The result (not shown) shows that this shear forcing case also produces a burst of convection. Again, the outward propagation of inertia-gravity waves emanating from the convection can produce LLJs. In short, the entire evolution scenario of cloud resembles that of the counter part confluent case (Fig. 4), except that the convection is advected

leftward by the prevailing negative geostrophic wind ($u_g < 0$) that is specified below 12 km by the spinup procedure.

With the inclusion of the along front moisture gradient ($\partial q_v/\partial y$), a long lasting convective system is produced. Fig. 11 shows the cloud profile and wind vectors at t = 46 hrs. Unlike the confluent case (Fig. 8b), this case does not produce visible slantwise convection. The presence of the positive shear of the geostrophic wind ($\partial u_g/\partial z > 0$) may be the reason for the suppression of the slantwise convection. By examining Fig. 11, a prominent feature can be identified. There is a main circulation generated at mid- to upper levels (5 to 15 km) on the right side of the upright convection. The return branch of this circulation intercepts the cloud at mid levels. In contrast, the return branch of the same circulation of the confluent case (Fig. 8b) can extend to the bottom of the atmosphere and intercept the cloud at low-levels. By examining Chen et al. al's (1996) result, it is not difficult to find that their convective system produced not only the low-level but also the mid-level return flow on the right side of the upright cloud. Therefore, it is suggested that the contribution due to shear forcing in their simulation can also be important.

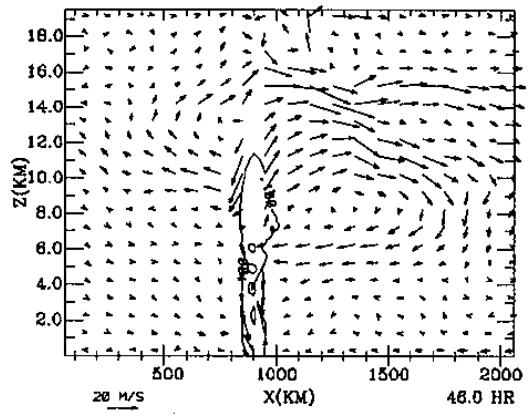

Figure 11: *As in Fig. 8 except for the case with shear frontal forcing at t = 46 hrs.*

4 Summary

We used a two-dimensional, nonhydrostatic model to demonstrate how the ageostrophic circulation associated with the upper-level front can trigger convection and lead to the development of the LLJ. Two types of frontal forcing were applied in the sensitivity experiments. The first was confluent forcing while the second was shear forcing. Instead of solving the traditional Sawyer-Eliassen equation, we gradually increased the frontal forcing over a period of 12 hours. During the spinup, we did not observe the production of inertia-gravity waves.

Our numerical experiments show that the secondary circulation induced by the frontal forcing can be explained by the thermal wind adjustment process. The rising and sinking motion of the circulation can be diagnosed by the convergence and divergence of the Q vector as discussed by Hoskins et al. (1978). By introducing a moisture pool at low-levels, the ageostrophic secondary circulation was able to induce convection. Once the convection developed, internal gravity waves were generated and propagated away from the center of the convection. We further examined main characteristics of internal gravity waves against the linear wave theory by conducting comprehensive tests using a time independent diabatic heat source. Our result is in a good agreement with the analytic solution.

From our study, we found that the dominant mode of internal gravity waves is determined by the depth of the heating profile. This dominant mode (n=2) is manifested by the presence of rotors and solitary waves. The development of the LLJ is associated with the outward propagation of rotors. The Coriolis turning of the lower branch circulation of the rotor can lead to the generation as well as the outward expansion of the LLJ.

The LLJ is important for advecting moist air to sustain convection. Without the inclusion of the along frontal moisture gradient ($\partial q_v/\partial y$), the convection is developed in a burst mode with a time scale of about 20 - 30 hrs. Since no additional moisture can be replenished, the exhaustion of the CAPE is the main reason to cause the burst development of the cloud. In contrast, a long lasting system is produced with the inclusion of ($\partial q_v/\partial y$).

The mid- to low-level slantwise convection and the tilting of the LLJ, found in the confluent frontal forcing case, has a structure similar to that from the 3D simulation using real data as reported by Chen et al. (1996). By interacting with the LLJ and the moisture gradient $\partial q_v/\partial y$, the environment becomes favorable to produce new convection to the right side of the upright convection than that to the left side. Because of the subsidence imposed by the existing upright convection, the new convection is usually shallow. Since the initial development of the LLJ can flaten the absolute momentum surface at low-levels, the newly developed shallow convection tends to be merged with its neighboring deep upright convection due the reduction of the inertia resistant force in the horizontal direction. The resulting manifestation of these processes is the generation of the slantwise convection.

Our shear frontal forcing case does not generate the slantwise convection. The lack of the slantwise cloud component is caused by the appearance of the

positive geostrophic wind shear ($\partial u_g/\partial z > 0$), when the along front temperature gradient ($\partial\theta/\partial y$) is spun up as a part of the model's reference state. Because of the presence of this positive wind shear, the upright convection and the newly developed shallow convection to its right side will be merged together promptly. This results in producing a main and long lasting deep upright convective system.

Acknowledgments. This work was sponsored by NASA Headquarters under RTOP 460-23-53-20. Our sincere appreciation also goes to Craig Bishop for his important role in the development of the frontal spinup procedure. Special thanks also go to Drs. R. F. Adler and R. Kakar for their support of this research.

5 References

Chen, C., 1991: A nested-grid, non-hydrostatic, elastic model using a terrain-following coordinate transformation: The radiative-nesting boundary conditions. *Mon. Wea. Rev.*, **119**, 2852-2869.

Chen, C, W.-K. Tao, P.-L. Lin, G. S. Lai, S.-F. Tseng, and T.-C. Chen Wang, 1996: The intensification of the low-level jet in the development of mesoscale convective systems in a Mei-Yu front. *Mon. Wea. Rev.*, accepted pending revision.

Chen, Q., 1982: The instability of the gravity-inertia wave and its relation to low-level jet and heavy rainfall. *J. Meteor. Soc. Japan*, **60**, 1041-1057.

Chen, X. A., and Y.-L. Chen, 1995: Development of low-level jets during TAMEX. *Mon. Wea. Rev.*, **123**, 1695 - 1719.

Chen, Y.-L., X. A. Chen, and Y.-X. Zhang, 1994: A diagnostic study of the low-level jet during TAMEX IOP 5. *Mon. Wea. Rev.*, **122**, 2257 - 2284.

Chou, L. C., C. P. Chang, and R. T. Williams, 1990: A numerical simulation of the Mei-Yu front and the associated low level jet. *Mon. Wea. Rev.*, **118**, 1408 - 1428.

Eliassen, A., 1962: On the vertical circulation in frontal zones. *Geofys. Publ.*, **24** (4), 147 - 160.

Hoskins, B. J., I. Draghici, and H. C. Davies, 1978: A new look at the ω-equation. *Quart. J. Roy. Meteor. Soc.*, **104**, 31-38.

Hsu, W.-R., and W.-Y. Sun, 1994: A numerical study of a low-level jet and its accompanying secondary circulation in a Mei-Yu system. *Mon. Wea. Rev.*, **122**, 324 - 340.

Keyser, D., and M.A. Shapiro, 1986: A review of the structure and dynamics of upper-level frontal zones. *Mon. Wea. Rev.*, **114** 452 - 499.

Mapes, B., 1993: Gregarious tropical convection. *J. Atmos. Sci.*, **50**, 2026-2037.

Matsumoto, S., 1973: Lower tropospheric wind speed and precipitation activity. *J. Meteor. Soc. Japan*, **51**, 101-107.

Ninomiya, K., and T. Akiyama, 1974: Band structure of mesoscale clusters associated with low-level jet stream. *J. Meteor. Soc. Japan*, **52**, 300-313.

Orlanski, I., and R.B. Ross, 1977: The circulation associated with a cold front. Part I: Dry case. *J. Atmos. Sci.*, **34**, 1619 - 1633.

Reeder, M.J., and R.K. Smith, 1987: A study of frontal dynamics with application to the Australian summertime "cool change". *J. Atmos. Sci.*, **44**, 687 - 705.

Rottman, J. W., and F. Einaudi, 1993: Solitary waves in the atmosphere. *J. Atmos. Sci.*, **50**, 2116-2136.

Sawyer, J.S., 1956: The vertical circulation at meteorological fronts and its relation to frontogenesis. *Proc. Roy. Soc. London*, **A234**, 346 - 362.

Tao, W.-K., and S.-T. Soong, 1986: A study of the response of deep tropical clouds to mesoscale processes: Three-dimensional numerical experiments. *J. Atmos. Sci.*, **43**, 2653-2676.

_____ ,and J. Simpson, 1993: Goddard cumulus ensemble model. Part I: Model description. *Terrestrial, Atmospheric and Oceanic Sci.*, **4**, 35-72.

Wang, T.-A., Y.-L. Lin, H.F.M. Semazzi, and G.S. Janowitz, 1996: Response of a stably stratified atmosphere to large-scale diabatic forcing with applications to wind patterns in Brazil and the Sahel. *J. Geophys. Res.*, **101**, 7049-7073.

Uccellini, L. W., and D. R. Johnson, 1979: The coupling of upper and lower tropospheric jet streaks and implications for the development of severe convective storms. *Mon. Wea. Rev.*, **107**, 682-703.